BIOCHEMISTRY
including biophysical chemistry & molecular biology
Article

Biochemistry **2009,** *48,* 11319–11328 11319
DOI: 10.1021/bi901244f

Calmodulin Is a Nonessential Activator of Secretory Phospholipase A_2[†]

Lidija Kovačič,[‡] Marko Novinec,[§] Toni Petan,[‡] Antonio Baici,[∥] and Igor Križaj*[,‡]

[‡]*Department of Molecular and Biomedical Sciences and* [§]*Department of Biochemistry and Molecular and Structural Biology, Jožef Stefan Institute, Ljubljana, Slovenia, and* [∥]*Department of Biochemistry, University of Zürich, Zürich, Switzerland*

Received July 21, 2009; Revised Manuscript Received October 1, 2009

ABSTRACT: Ammodytoxins are presynaptically neurotoxic snake venom group IIA secreted phospholipase A_2 enzymes that interact specifically with calmodulin in the cytosol of nerve cells. We show that calmodulin behaves as an activator of ammodytoxin under both nonreducing and reducing (cytosol-like) conditions by stimulating its enzymatic activity up to 21-fold. Kinetic analysis, using a general modifier mechanism, and surface plasmon resonance measurements reveal that calmodulin influences both the catalytic and the vesicle binding properties of the enzyme without affecting its calcium binding properties. The equilibrium dissociation constant of the ammodytoxin−calmodulin complex under cytosol-like conditions is in the low nanomolar range (3 nM), while under nonreducing conditions, the binding affinity is in the subnanomolar range (0.07−0.18 nM). Upon exposure to cytosol-like conditions, ammodytoxin undergoes a slow hysteretic transition to a less active state. Calmodulin stabilizes the conformation of ammodytoxin and thereby restores its activity. These results provide insights into the neurotoxic action of ammodytoxins and the mechanisms involved in the regulation of secreted phospholipase A_2 activity within the cytosol.

Secreted phospholipase A_2 enzymes (sPLA$_2$s,[1] EC 3.1.1.4) are relatively small (13−19 kDa), Ca^{2+}-dependent, disulfide-rich enzymes that hydrolyze the *sn*-2 ester bond of glycerophospholipids to release lysophospholipids and fatty acids (*1*). The enzymatic activity of these proteins is basic for many of the physiological and pathological activities that they exert. In mammals, 10 different sPLA$_2$ isoenzymes are implicated in processes from innate immunity to cell proliferation and from inflammatory diseases to cancer (*2*). Animal venoms, and snake venoms in particular, are rich sources of these enzymes, and some of the most potent neurotoxins, myotoxins, and anticoagulants have been characterized (*3*). Ammodytoxins (Atxs) and ammodytin I_2 (AtnI_2) are group IIA (GIIA) sPLA$_2$s from the venom of the most venomous European snake *Vipera ammodytes ammodytes* (*4*, *5*). They are structurally very similar to their mammalian homologues. While AtnI_2 is devoid of toxic activity, Atxs are potent presynaptic neurotoxins. They paralyze the neuromuscular junction by a process in which the phospholipase activity is essential (*6*).

Secreted PLA$_2$s have been extensively studied as a paradigm for interfacial enzymology (*7*). To gain access to their water-insoluble phospholipid substrates, sPLA$_2$s bind to the lipid−water interface along their interfacial binding surface, a group of 10−20 residues forming a relatively flat surface that surrounds the entrance to the active site and covers 20−40 phospholipid molecules (*2*). The membrane binding step is kinetically and structurally distinct from the subsequent catalytic events at the active site, which include binding of a single phospholipid molecule, chemical substrate hydrolysis, and release of products (*8*). Ca^{2+} is an essential cofactor for substrate binding at the active site and for catalysis (*8*, *9*), but not for adsorption of sPLA$_2$s to the membrane (*10*). The overall substrate specificity of sPLA$_2$s is controlled by two separate factors: the binding affinity of the enzyme for different membrane surfaces and the relative velocity of the hydrolysis of different substrates by the membrane-bound enzyme (*11*). Most sPLA$_2$s bind to anionic phospholipid vesicles with very high (subpicomolar) affinity, which eliminates the first kinetic event (the membrane binding step) and enables a scooting mode of catalysis in which the enzyme undergoes many successive turnover cycles without leaving the interface. This has provided the basis for the extension of Michaelis−Menten solution kinetics to interfacial enzymology (*7*).

Besides the range of various organic compounds that are potent inhibitors of sPLA$_2$s, there are several mammalian and snake venom high-affinity sPLA$_2$-binding proteins that inhibit their enzymatic, and toxic, activity (*2*). Some peptide/protein activators of sPLA$_2$s are known, e.g., melittin (*12*) and phospholipase A_2-activating protein (PLAA) (*13*). The sPLA$_2$ activation effect of melittin, and probably also of PLAA, which possesses a melittin-like structural element, is however based on its interaction with phospholipids (*14*).

Calmodulin (CaM) regulates numerous physiological processes inside the cytosol of animal cells in a Ca^{2+}-dependent manner (*15*, *16*). Phospholipase A_2 enzymes have been reported to be activated by direct interaction with CaM (*17*, *18*). Here we report that CaM, by high-affinity binding to Atxs, significantly

[†]This work was supported by Grant P1-0207 from the Slovenian Research Agency.

*To whom correspondence should be addressed: Jamova 39, SI-1000 Ljubljana, Slovenia. Telephone: +386-1-477-3713. Fax: +386-1-477-3594. E-mail: igor.krizaj@ijs.si.

[1]Abbreviations: AtnI_2, ammodytin I_2; AtxA and AtxC, ammodytoxins A and C, respectively; BSA, bovine serum albumin; CaM, calmodulin; DAUDA, 11-dansylundecanoic acid; DTPC and DTPG, 1,2-ditetradecyl-*sn*-glycero-3-phosphocholine and -glycerol, respectively; FABP, fatty acid-binding protein; HBSS, Hanks' balanced salt solution; Hepes, *N*-(2-hydroxyethyl)piperazine-*N*-2-ethanesulfonic acid; PC, phosphocholine; PG, phosphoglycerol; POPC and POPG, 1-palmitoyl-2-oleoyl-*sn*-glycero-3-phosphocholine and -glycerol, respectively; PyPG, 1-hexadecanoyl-2-(1-pyrenedecanoyl)-*sn*-glycero-3-phosphoglycerol; RU, response units; RFU, relative fluorescence units; sPLA$_2$, secreted phospholipase A_2; SPR, surface plasmon resonance.

Published on Web 10/19/2009

increases their resistance to cytosol-like conditions and potentiates their enzymatic activity. Kinetic analysis of the Atx−CaM interaction under nonreducing and cytosol-like conditions shows that CaM stabilizes these $sPLA_2$s in the reducing environment and stimulates their phospholipase activity as a nonessential activator, in a manner independent of the redox potential of the solvent. Stabilization of $sPLA_2$s and stimulation of their enzymatic activity in specific cellular compartments offer a possible interpretation of the neuropathological effects produced by Atxs following their internalization into the cytosol of the nerve cell (*19*−*21*).

EXPERIMENTAL PROCEDURES

Materials. Ammodytoxins A and C (AtxA and AtxC, respectively) and $AtnI_2$ were purified from *Vipera a. ammodytes* venom, and the AtxA(F24W) mutant was produced as described previously (*22*, *23*). Hog brain CaM was obtained from Boehringer Mannheim. 11-Dansylundecanoic acid (DAUDA), 1-palmitoyl-2-oleoyl-*sn*-glycero-3-phosphocholine and -glycerol (POPC and POPG, respectively) and 1,2-ditetradecyl-*sn*-glycero-3-phosphocholine and -glycerol (DTPC and DTPG, respectively) were from Avanti Polar Lipids. Fatty acid-free bovine serum albumin (BSA), *N*-(2-hydroxyethyl)piperazine-*N*-2-ethanesulfonic acid (Hepes), and glutathione (reduced and oxidized forms) were purchased from Sigma. Hanks' balanced salt solution (HBSS) and 1-hexadecanoyl-2-(1-pyrenedecanoyl)-*sn*-glycero-3-phosphoglycerol (PyPG) were from Invitrogen. The bacterial expression plasmid encoding rat liver fatty acid-binding protein (FABP) was a generous gift from D. C. Wilton (University of Southampton, Southampton, U.K.), and the recombinant protein was prepared as described previously (*24*). All other chemicals were of at least analytical grade and were purchased from Sigma and Serva.

Interfacial Kinetic Studies with Pyrene-Labeled Phospholipid Vesicles. Phospholipolytic activities of $sPLA_2$s were measured using a modification of the sensitive fluorimetric assay originally described by Radvanyi (*25*, *26*). CaM and $sPLA_2$ were mixed at different molar ratios and preincubated in different assay buffers for fixed time intervals. Three different assay buffers were used: (A) 50 mM Tris-HCl (pH 7.4), 50 mM KCl, and 1 mM $CaCl_2$, (B) 50 mM Tris-HCl (pH 7.4), 18 mM NaCl, 135 mM KCl, and 20 μM $CaCl_2$, containing 9.86 mM glutathione in reduced form and 0.14 mM glutathione in oxidized form (reducing, cytosol-like conditions) (*27*), and (C) 50 mM Tris-HCl (pH 7.4), 18 mM NaCl, 135 mM KCl, and 1 mM $CaCl_2$, containing 9.86 mM glutathione in reduced form and 0.14 mM glutathione in oxidized form (reducing, cytosol-like conditions with 1 mM Ca^{2+}). The final enzyme concentration in the reaction mixture was 0.25 or 2.5 nM for $AtnI_2$ and ranged from 0.041 to 2.5 nM for AtxA and from 0.17 to 2.5 nM for AtxC. All $sPLA_2$ dilutions were prepared just prior to use in assay buffer containing 0.06% (w/v) BSA to prevent loss of enzyme activity by adsorption to the walls of the test tube (*26*). Small unilamellar vesicles composed of PyPG were prepared as described previously (*26*). The final phospholipid concentration in the assays was 1.4 μM, except for the kinetic measurements aimed at demonstrating the activation mechanism, where the total phospholipid concentrations ranged from 0.06 to 2.2 μM. The final concentration of BSA in the assays was 0.06% (w/v). Fluorescence was measured at 25 °C in 96-well plates on a Safire2 microplate reader (Tecan), with excitation and emission wavelengths set to 342 and 395 nm, respectively. Typically, 19 kinetic cycles were performed with 10 flashes per well and an integration time of 40 μs. Alternatively, the assay was performed in quartz cuvettes with magnetic stirring at 25 °C using a LS50B spectrofluorimeter (Perkin-Elmer). Cuvettes were thoroughly washed with 0.1 M HCl after each measurement. Background fluorescence was subtracted, and initial reaction velocities (v_i) were calculated from the slopes of the progress curves. Values of "K_m", corresponding to the total phospholipid concentration required for the half-limiting rate, were determined by nonlinear regression fitting of the Michaelis−Menten equation to reaction velocities versus phospholipid concentration. As discussed below in Theoretical Background and Analysis of Kinetic Data, this value must be interpreted as an apparent dissociation constant, $K_{d(app,kin)}$. These and following calculations were performed with GraphPad Prism version 5.02 for Windows from GraphPad Software (San Diego, CA).

Interfacial Kinetics with Vesicles Composed of Nonmodified Phospholipids. The rate of hydrolysis of large unilamellar vesicles, containing POPC or 10 mol % POPG in POPC, by $sPLA_2$s was determined by monitoring the displacement of a fluorescent fatty acid analogue, DAUDA, from FABP as described previously (*28*, *29*). CaM and AtxC were preincubated at different molar ratios (from 0.1 to 30) for 20 min in buffer B. Final enzyme concentrations in the reaction mixture were 0.28, 2.8, and 65 nM for POPG, 10 mol % POPG in POPC vesicles, and POPC vesicles, respectively. Assays were performed in a final volume of 1.3 mL and contained 30 μM total phospholipid, 1 μM DAUDA, and 10 μg of recombinant FABP. The fluorescence was monitored in acrylic fluorimetric cuvettes at 37 °C with constant magnetic stirring on a C61 Photon Technology International fluorimeter with excitation and emission wavelengths set to 350 and 500 nm, respectively. As typically observed in assays with phospholipases, reaction traces deviated from linearity. Therefore, after subtraction of the baseline fluorescence, initial rates were calculated by fitting a cubic polynomial in time (t) (eq 1) to experimental traces:

$$F = at^3 + bt^2 + ct + d \quad (1)$$

where F is the emitted fluorescence. Initial rates corresponded to the first derivatives of this polynomial for $t = 0$.

Ca^{2+}-Affinity Studies. The dependence of the initial rate of hydrolysis of phospholipid vesicles by AtxC (0.625 nM) on the concentration of free Ca^{2+} in the presence and absence of CaM (31.25 nM) was determined using the PyPG assay described above. Buffered solutions containing increasing amounts of free Ca^{2+} were prepared in HBSS without Ca^{2+} and Mg^{2+} containing 20 μM EGTA (*30*). The apparent Ca^{2+} dissociation constants [$K_{Ca(app)}$] of AtxC in the presence or absence of CaM were obtained by fitting a binding hyperbola to experimental data (*30*).

Intrinsic Fluorescence Measurements. The effect of CaM on the stability of Atx under reducing conditions was determined by measurements of intrinsic tryptophan fluorescence of the AtxA(F24W) mutant [the wild-type Atxs (A, B, or C) do not possess a Trp residue]. The mutant (100 nM) was preincubated for 1 h at room temperature under nonreducing or reducing conditions in the presence or absence of 100 nM CaM. The samples were incubated in HBSS supplemented with 20 μM EGTA and 520 μM Ca^{2+} in the presence or absence of 9.86 mM reduced glutathione and 0.14 mM oxidized glutathione. Trp emission spectra (300−420 nm) were recorded on a Perkin-Elmer

Scheme 1

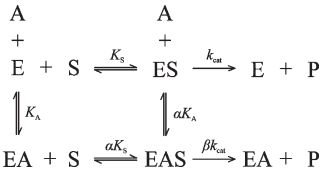

LS50B fluorimeter with an excitation wavelength of 280 nm. Appropriate blanks were recorded separately and subtracted from the spectra.

Theoretical Background and Analysis of Kinetic Data. The general modifier mechanism (*31*) was used to describe the interaction between Atx (E) and CaM (A) in the presence of substrate (S) (Scheme 1), where K_S and K_A are the corresponding dissociation constants, k_{cat} is the catalytic constant for the conversion of S to product P, and α and β are dimensionless coefficients. For this model, the reaction rate in the presence of activator A, v_A, is given by eq 2:

$$\frac{v_A}{v_0} = \frac{(1+\sigma)\left(1+\beta\frac{[A]}{\alpha K_A}\right)}{\sigma\left(1+\frac{[A]}{\alpha K_A}\right)+1+\frac{[A]}{K_A}} \quad (2)$$

where v_0 is the reaction velocity in the absence of CaM and σ is $[S]/K_m$. K_m has the same dimensions as the phospholipid concentration, independent of how the latter is expressed, and σ is a pure number. This K_m value must be interpreted as an apparent dissociation constant, $K_{d(app,kin)}$, for dissociation from the interface and is valid only under the particular kinetic assay conditions used here. The derivation of eq 2 is based on the assumption of a quasi-equilibrium for the binding of A to E and ES, and of a steady state for the fluxes around ES and EAS. The validity of these assumptions was discussed by Topham and Brocklehurst (*32*).

To investigate the mechanism of Atx activation by CaM, we used the specific velocity plot (*33*). In this representation, eq 2 is rewritten as

$$\frac{v_0}{v_A} = \frac{[A]\left(\frac{1}{\alpha K_A}-\frac{1}{K_A}\right)}{1+\beta\frac{[A]}{\alpha K_A}}\frac{\sigma}{1+\sigma}+\frac{1+\frac{[A]}{K_A}}{1+\beta\frac{[A]}{\alpha K_A}} \quad (3)$$

where v_0 and v_A are reaction rates in the absence and presence of modifier A, respectively. Data collected at different concentrations of CaM and substrate were plotted as v_0/v_A versus $\sigma/(1+\sigma)$, giving a family of straight lines. The intercepts of the graphically extrapolated lines at abscissa = 0 (intercept *a*) and abscissa = 1 (intercept *b*) were replotted as $a/(a-1)$ and $b/(b-1)$, respectively, versus $[A]^{-1}$. From these replots, the α and β coefficients were determined as described by Baici (*33*).

Surface Plasmon Resonance (SPR) Analysis. Binding of Atx to phospholipid vesicles was evaluated by SPR on a Biacore X instrument (Biacore AB, Uppsala, Sweden) as described previously (*34*). Large unilamellar vesicles of nonhydrolyzable DTPG and DTPC phospholipids were prepared by extrusion in SPR flow buffer [10 mM Hepes (pH 7.4), 150 mM NaCl, and 0.5 mM $CaCl_2$] and immobilized on a Pioneer L1 sensor chip (*35*). The amount of vesicles coated on the chip corresponded to 5900 response units (RU) for DTPG and 6200 RU for DTPC vesicles. Nonspecific binding sites on the chip were saturated by five consecutive injections of 60 μL of 0.3 mg/mL BSA in flow buffer at 60 μL/min, which typically led to an increase in the magnitude of the signal of approximately 1000 RU. AtxC, alone (50 nM) or in the presence of CaM (5, 50, or 500 nM), was preincubated in SPR buffer for 10 min. AtxC, CaM, or AtxC−CaM solutions were injected over the sensor chip at 25 °C with a high flow rate of 60 μL/min to minimize mass transport effects. Association was monitored for 60 s and dissociation for 3 min (*34*, *35*). The immobilized lipid surface was regenerated between subsequent measurements via injection of 60 μL of 50 mM NaOH.

RESULTS

Effect of CaM on the Phospholipase Activity of Atxs. The apparent rates of hydrolysis of small unilamellar vesicles, composed of anionic PyPG, by AtxA, AtxC, and $AtnI_2$, were determined following preincubation with different concentrations of CaM for 40 min under nonreducing (Figure 1A) or reducing, cytosol-like (Figure 1B) conditions. The plots displayed hyperbolic profiles typical of saturation binding. Under nonreducing conditions, AtxA and AtxC displayed, maximally, 5- and 3-fold increases in the rate of hydrolysis of PyPG vesicles in the presence of CaM. These maximal increases were significantly higher under cytosol-like conditions, up to 21- and 14-fold higher values being observed for AtxA and AtxC, respectively. In contrast, regardless of the incubation conditions, CaM did not affect the enzymatic activity of $AtnI_2$, an Atx homologue that possesses no affinity for CaM (*36*). Thus, the increase in the enzymatic activity of Atxs in the presence of CaM appears to depend on the specific association of the two proteins.

To ascertain that this effect is not due to particular characteristics of the PyPG substrate or the assay setup, an alternative phospholipase assay was used, based on the differential binding affinity of FABP for free fatty acids, which is not limited by the use of a particular type of phospholipid substrate. Both phospholipase activity assays gave almost identical results. Atxs, like most other $sPLA_2$s, exhibit a significantly higher affinity for binding to anionic than to zwitterionic phospholipid membranes, resulting in differences of up to 3 orders of magnitude in their rate of vesicle hydrolysis (*29*, *37*). We therefore examined the influence of vesicle composition, i.e., their surface charge, on activation in the presence of CaM. Extruded large unilamellar vesicles, composed of pure anionic POPG, zwitterionic POPC, or a 10 mol % mixture of POPG in POPC, were used as substrates. The results in Figure 1C show that a several-fold increase in AtxC enzymatic activity was observed with all vesicle types, following preincubation of AtxC with CaM under cytosol-like conditions. The increase in the phospholipase activity of AtxC on pure POPG was 5-fold at a CaM:AtxC concentration ratio of 30. Because of the low activity of AtxC on POPC-rich substrates, much higher concentrations of $sPLA_2$ were necessary for accurate measurements; therefore, the high CaM:AtxC concentration ratios used in measurements with POPG vesicles could not be achieved (4.6 and 14 for POPC and POPG/POPC, respectively). Nevertheless, the potentiation of enzyme activity was even higher: 10-fold on mixed POPG/POPC vesicles and 7-fold on pure POPC vesicles.

Effect of CaM on the Ca^{2+}-Binding Affinity of Atx. To verify whether the Ca^{2+}-affinity of Atx is altered on binding to CaM, we measured the enzymatic activity of AtxC on PyPG vesicles as a function of the concentration of free Ca^{2+} ions (*7*, *37*, *38*). The $K_{Ca(app)}$ values obtained in the absence and presence of CaM were 31 ± 9 and 29 ± 7 μM, respectively (Figure 2), demonstrating that binding to CaM did not affect the apparent affinity of AtxC for Ca^{2+}.

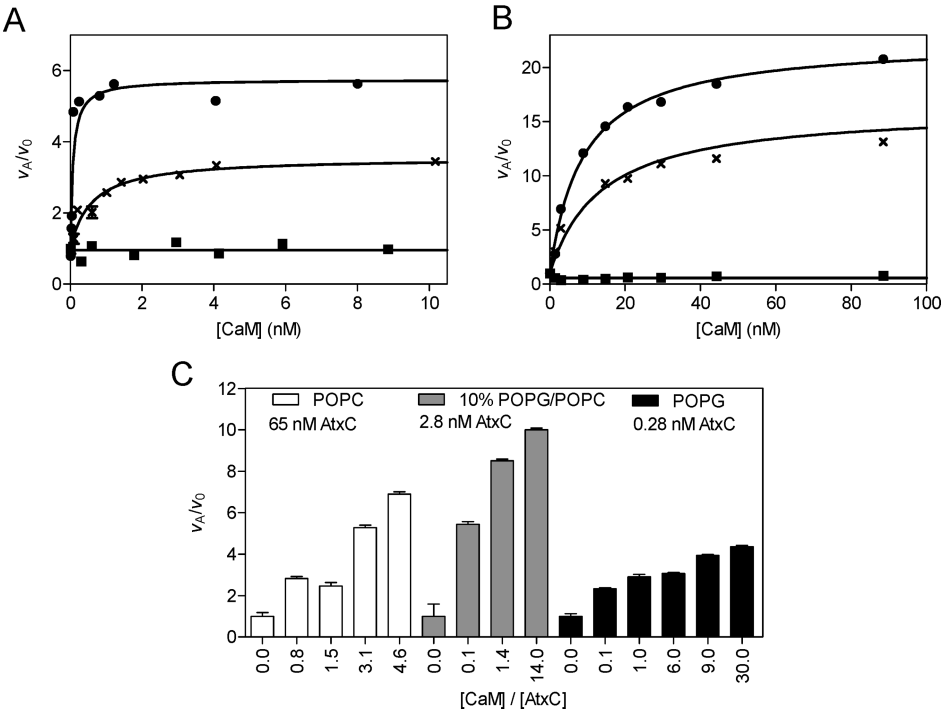

FIGURE 1: Activation of Atxs by calmodulin. (A) The initial rates of hydrolysis of PyPG vesicles by 0.041 nM AtxA (●), 0.24 nM AtxC (×), and 0.25 nM $AtnI_2$ (■) in the absence (v_0) or presence (v_A) of a range of concentrations of CaM were determined from the reaction progress curves and plotted as v_A/v_0 vs CaM concentration. All samples were incubated in a nonreducing environment [50 mM Tris-HCl (pH 7.4), 50 mM KCl, and 1 mM $CaCl_2$] for 40 min prior to the measurement. A rectangular hyperbolic function was fitted to the data. (B) Ratios of the initial rates of hydrolysis of PyPG vesicles by 2.5 nM AtxA (●), 1 nM AtxC (×), and 2.5 nM $AtnI_2$ (■) in the presence (v_A) and absence (v_0) of CaM. All samples were incubated in a reducing, cytosol-like environment for 40 min [50 mM Tris-HCl (pH 7.4), 18 mM NaCl, 135 mM KCl, 20 μM $CaCl_2$, 9.86 mM reduced glutathione, and 0.14 mM oxidized glutathione] prior to the measurement. (C) The rates of hydrolysis by AtxC of POPC, POPG, and 10 mol % POPG in POPC vesicles in the presence of different concentrations of CaM were determined by the FABP assay. All samples were preincubated in a cytosol-like environment for 20 min prior to measurement. The initial rates of hydrolysis were determined from the initial slopes of the progress curves and plotted as v_A/v_0.

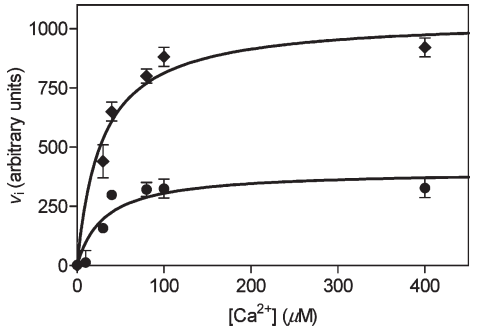

FIGURE 2: Binding of AtxC to CaM does not affect the apparent affinity of AtxC for Ca^{2+}. The dependence of the initial reaction velocities of PyPG vesicle hydrolysis by AtxC on the concentration of free Ca^{2+} ions in the presence (◆) and absence (●) of CaM was determined. Both profiles were fitted by a hyperbolic binding equation, and the calculated $K_{Ca(app)}$ values were 31 ± 9 μM for AtxC and 29 ± 7 μM for AtxC preincubated with CaM.

Effect of CaM on the Stability of Atx under Reducing Conditions. The enzymatic activity of AtxA has been shown to be reduced to 60% of the initial value after incubation for 5 min in a reducing environment similar to the cytosolic one but then remained practically constant during incubation for a further 55 min (*39*). We explained this finding by the reduction of the most sensitive disulfide bonds in the $sPLA_2$ molecule, resulting in structural alterations that still enable phospholipid hydrolysis, but at a lower rate. Here we have extended our analysis of the effect of cytosol-like conditions on the activity of AtxA in the presence of CaM. As shown in panels A and C of Figure 3, the rate of PyPG vesicle hydrolysis by AtxA was gradually reduced to ~50% after exposure of the toxin to reducing conditions for 60 min or more. The process was reversible, since transferring the $sPLA_2$ from reducing to nonreducing conditions again restored its activity (Figure 3D). The presence of CaM during the incubation of AtxA under reducing conditions, however, completely prevented the loss of AtxA enzymatic activity, even when it was assayed under reducing conditions (Figure 3C). Moreover, addition of CaM completely restored the enzymatic activity of AtxA after a 2 h preincubation of the toxin in reducing buffer (Figure 3B).

Effect of CaM on the Conformational Stability of Atx. To gain further insight into the stabilizing effect of CaM on Atx under reducing conditions, we analyzed the fluorescence emission spectra of the AtxA(F24W) mutant. The wild-type Atxs (A, B, and C) do not possess a Trp residue, and the replacement of Phe by Trp at position 24 in AtxA only marginally affected its affinity for CaM (*23*). The fluorescence emission spectrum of AtxA(F24W) recorded in the presence of 0.5 mM Ca^{2+} displayed a Trp fluorescence emission maximum at 360 nm (Figure 4). The presence of reduced glutathione in the buffer caused a slight decrease in the signal intensity and a shift in the emission maximum toward 380 nm, reflecting a considerable conformational change in the structure of AtxA(F24W) in the vicinity of Trp24. On the other hand, binding of CaM to AtxA(F24W) caused an increase in the signal intensity of ~50% but no change in the Trp fluorescence emission maximum in nonreducing buffer. Most importantly, upon exposure of the complex to the reduced form of glutathione, no shift in the emission maximum

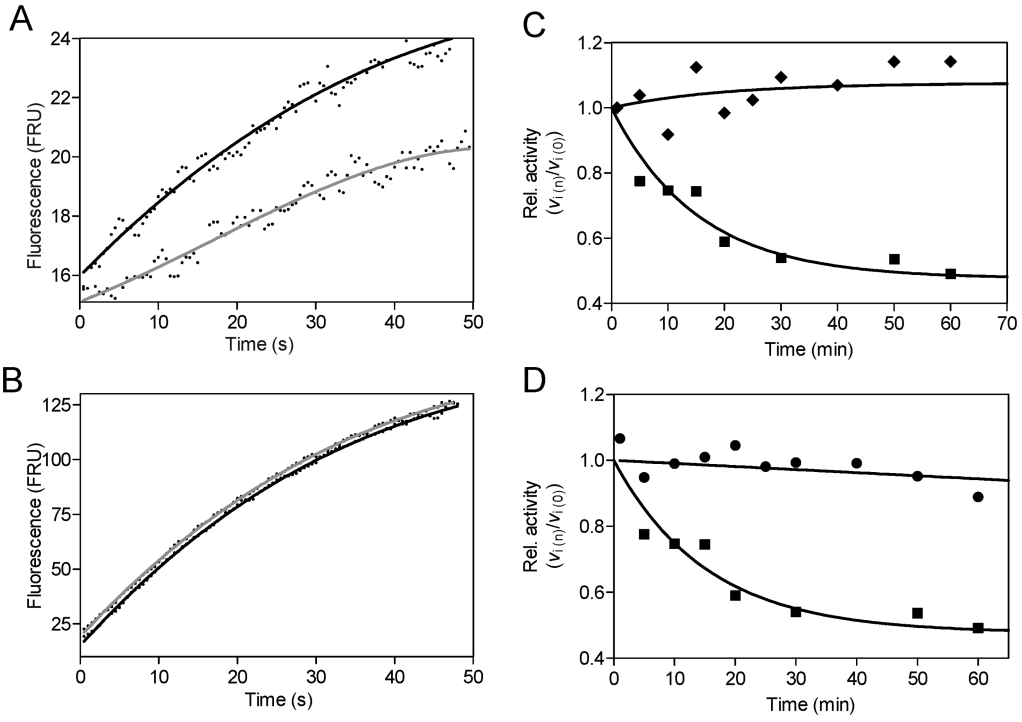

FIGURE 3: CaM reduces the loss of Atx activity in a reducing environment. Incubations and phospholipase activity assays were performed under either nonreducing [50 mM Tris-HCl (pH 7.4), 18 mM NaCl, 135 mM KCl, and 1 mM $CaCl_2$] or reducing conditions [50 mM Tris-HCl (pH 7.4), 18 mM NaCl, 135 mM KCl, 1 mM $CaCl_2$, 9.86 mM reduced glutathione, and 0.14 mM oxidized glutathione]. All measurements were taken at 25 °C using 1.4 μM PyPG vesicles as the substrate. (A) Reaction progress curves for AtxA (0.08 nM) without preincubation (black line) and after preincubation for 2 h under reducing conditions (gray line). (B) Reaction progress curves of AtxA (0.08 nM) without preincubation (black line) and after preincubation for 2 h under reducing conditions, following the addition of 4 nM CaM just prior to the phospholipase activity measurement (gray line). (C) Ratio of the initial velocities of PyPG hydrolysis by AtxA (0.08 nM) in reducing buffer (v_i) at "n" and "0" min in the absence of CaM (■) to those in the presence of CaM (4 nM) (◆). AtxA and CaM were combined at time zero. (D) The initial velocity of PyPG hydrolysis by AtxA (0.08 nM) in the reducing buffer was measured at time n and compared to that at time zero (■). A comparison is made with the ratio of the initial velocities of the enzyme preincubated for the time (n) in reducing buffer before the activity assessment under the same conditions and the enzyme preincubated for the same time in reducing buffer but then transferred to the nonreducing buffer for the activity measurement (●). All values were normalized to the activity measured at time zero under the respective reaction conditions.

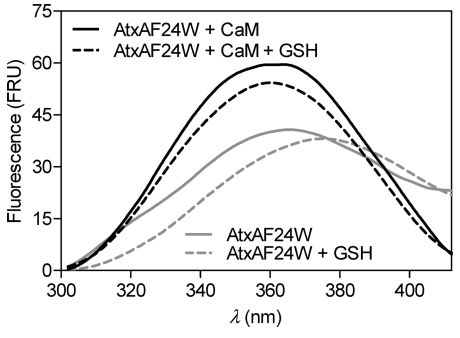

FIGURE 4: CaM increases the conformational stability of Atx in a reducing environment. Intrinsic tryptophan fluorescence emission spectra of the AtxA(F24W) mutant were recorded in a nonreducing environment (HBSS with 0.5 mM Ca^{2+}) and in a reducing environment (+GSH, HBSS with 0.5 mM $CaCl_2$, 9.86 mM reduced glutathione, and 0.14 mM oxidized glutathione), in the absence and presence of CaM (+CaM). Concentrations of AtxA(F24W) and CaM in the experimental mixtures were 100 nM. The excitation wavelength was 280 nm.

was observed, and the signal intensity was only slightly attenuated.

Mechanism of sPLA$_2$ Activation by CaM. Since the FABP assay is limited by the free fatty acid-binding capacity of FABP, the PyPG assay was chosen for a more detailed kinetic characterization of the influence of CaM on Atx activity. Measurements were performed under nonreducing conditions (buffer A described in Experimental Procedures) or under reducing, cytosol-like conditions (buffer C), with either AtxA or AtxC, over a range of substrate concentrations from 0.067 to 2.2 μM. Buffers A and C contained 1 mM Ca^{2+} to fully saturate CaM and Atx with this ion. The mechanism of Atx activation by CaM was analyzed with the specific velocity plot (*33*) based on eq 3. The effects of CaM on AtxA activity, under nonreducing and under reducing, cytosol-like conditions, are shown in Figure 5. The K_m value for AtxA under nonreducing conditions was 0.47 ± 0.37 μM and, for AtxC under cytosol-like conditions, 0.47 ± 0.19 μM (Figure 5A). This parameter is used here to calculate the dimensionless ratio $\sigma = [S]/K_m$. The primary specific velocity plot, v_0/v_A versus $\sigma/(1 + \sigma)$, gave straight lines with negative slopes intersecting on the negative side of the abscissa (Figure 5B, C). This is consistent with a nonessential activation mechanism with a combination of coefficients $\alpha > 1, \beta > 1$, and $\alpha \neq \beta$ in eqs 2 and 3. For nonessential activation, the value of α in the general modifier mechanism (Scheme 1) is coupled to the activation constant as αK_A. It is therefore not possible to calculate by nonlinear regression the individual values of α and K_A using eq 2. This problem can be circumvented by evaluating α independently, using the specific velocity method (eq 3), and using this value as a constant for fitting with eq 2.

The coefficients α and β and the dissociation constant K_A were calculated from the replots of $a/(a - 1)$ and $b/(b - 1)$ versus 1/[A], where a and b are the intercepts of the graphically extrapolated lines at abscissa = 0 (intercept a) and abscissa = 1 (intercept b),

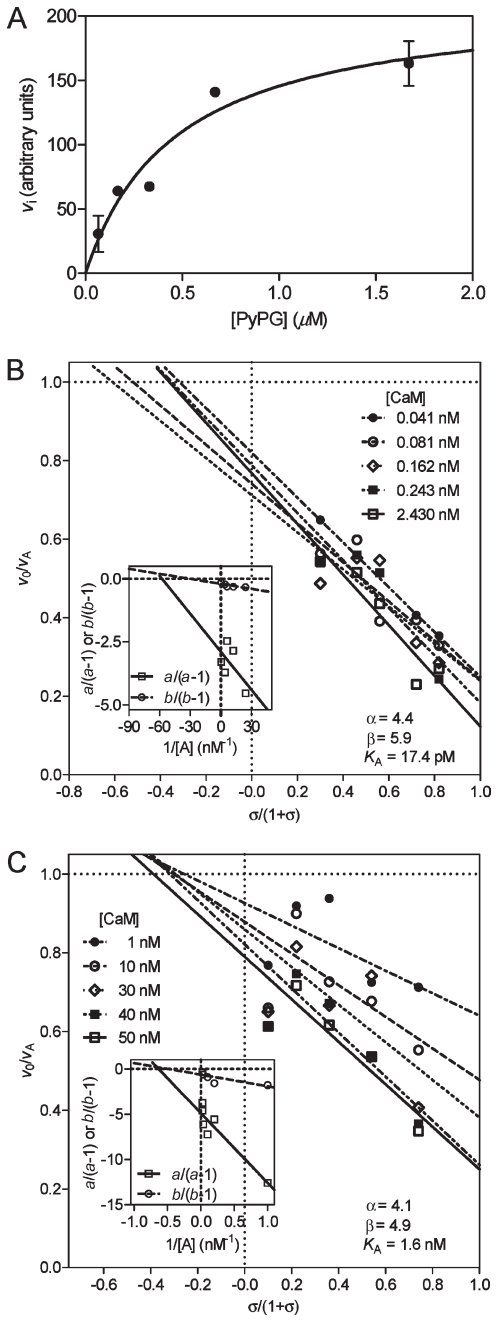

FIGURE 5: CaM is a nonessential activator of Atxs. (A) The equation for a rectangular hyperbola, equivalent to the Michaelis−Menten equation, was fitted to initial rates of hydrolysis of PyPG vesicles by AtxC as a function of the total phospholipid concentration. An apparent dissociation constant $K_{d(app,kin)}$ of 0.47 ± 0.19 μM was calculated as an analogue of K_m. (*B*) Activation of AtxA under nonreducing conditions [50 mM Tris-HCl (pH 7.4), 50 mM KCl, and 1 mM $CaCl_2$] and (C) activation of AtxC under reducing conditions [50 mM Tris-HCl (pH 7.4), 18 mM NaCl, 135 mM KCl, 1 mM $CaCl_2$, 9.86 mM reduced glutathione, and 0.14 mM oxidized glutathione]. The concentrations of AtxA and AtxC were 0.08 and 1 nM, respectively. Initial reaction velocities were measured at various CaM and total phospholipid concentrations, in the case of AtxA with 0.2, 0.4, 0.6, 1.2, and 2.2 μM PyPG and in the case of AtxC with 0.067, 0.167, 0.33, 0.67, and 1.67 μM PyPG. Initial reaction velocities were plotted as v_0/v_A vs $\sigma/(1+\sigma)$, where v_0 and v_A are initial reaction velocities in the absence and presence of CaM, respectively, and σ equals $[S]/K_m$ (eq 3). Intercepts of the extrapolated straight lines at $\sigma/(1+\sigma) = 0$ (a) and $\sigma/(1+\sigma) = 1$ (b) were replotted as $a/(a-1)$ and $b/(b-1)$ vs $[A]^{-1}$, respectively. Replots are shown as insets in the primary plots. From the replots, the parameter α and rough estimates of β and K_A were determined.

respectively, shown as insets in the primary plots in panels B and C of Figure 5. For the AtxC−CaM interaction under reducing conditions, we obtained the following values: $\alpha = 4.1$, $\beta = 4.9$, and $K_A = 1.6$ nM. For the AtxA−CaM interaction under nonreducing conditions, we obtained the following values: $\alpha = 4.4$, $\beta = 5.9$, and $K_A = 17.4$ pM. The purpose of the specific velocity plot was to determine the activation mechanism and to gather estimates of the parameters. The enzyme concentration in these experiments was relatively high, so the values of β and K_A are approximate because of the tight binding condition created by these artificial experimental conditions, which are nevertheless necessary for diagnostic purposes. However, the value of α is reliable because it can be obtained with precision from both slopes and intercepts in the specific velocity plot and its replot (*33*). This value will be used as a constant to refine calculations of β and K_A, using the procedure described in the next section.

Activation of Atxs by CaM under Different Redox Conditions. At a single concentration of the PyPG substrate (1.4 μM), we compared the binding of CaM to Atxs under nonreducing and reducing, cytosol-like conditions. In all cases, eq 2 was fitted to experimental data and the tight binding condition was circumvented by using a low enzyme concentration. The best-fit values of K_A, α, and β and the total enzyme concentration used in each experiment are shown in Figure 6. As stated above, to calculate K_A, the coefficient α was set constant in eq 2 using the values obtained from the specific velocity plot: $\alpha = 4.4$ for AtxA and $\alpha = 4.1$ for AtxC (Figure 5). For AtxA under nonreducing conditions, K_A was 72 pM and β was 13, while for AtxC, these parameters were 0.18 nM and 6.3, respectively. Under reducing conditions, K_A was 3.3 nM and β was 48 for AtxA and 3.3 nM and 12, respectively, for AtxC.

Binding of Atx to Phospholipid Vesicles. SPR analysis was performed to verify the surprising result from kinetic analysis that, in spite of activity stimulation of Atx on PG vesicles by CaM, the affinity of the complex for these vesicles is lower than the affinity of the enzyme alone. Measurements were performed on anionic DTPG and zwitterionic DTPC, nonhydrolyzable diether phospholipid vesicles, to prevent hydrolysis by $sPLA_2$ in the presence of Ca^{2+}. Although the ion is not required for the binding of $sPLA_2$ to the membrane surface, it is necessary for the formation of the Atx−CaM complex (*40*). CaM alone scarcely bound to any of the vesicles, as shown by the sensorgrams in panels B and D of Figure 7. From the qualitative appearance of the sensorgrams in Figure 7C, it is clear that the AtxC−CaM complex bound more effectively to zwitterionic DTPC vesicles than AtxC alone. In agreement with the results of the kinetic analysis, the effect was opposite on the negatively charged DTPG vesicles. In this case, the preincubation of AtxC with increasing concentrations of CaM resulted in a decrease in the SPR response (Figure 7A). According to the K_A value of ~0.18 nM, at 50 nM CaM ~94% of the AtxC molecules are complexed with CaM. If the affinity of the complex for the vesicles was similar to that of AtxC, the expected SPR response in the case of the complex would be approximately twice that in the case of AtxC, due to the approximately 2-fold higher molecular mass of the complex.

DISCUSSION

AtxA and AtxC differ only in two amino acid residues of 122 (*4*). They are highly active enzymes that result in very similar apparent rates of hydrolysis of anionic POPG vesicles, while on POPC zwitterionic phospholipid vesicles, AtxA is twice as active

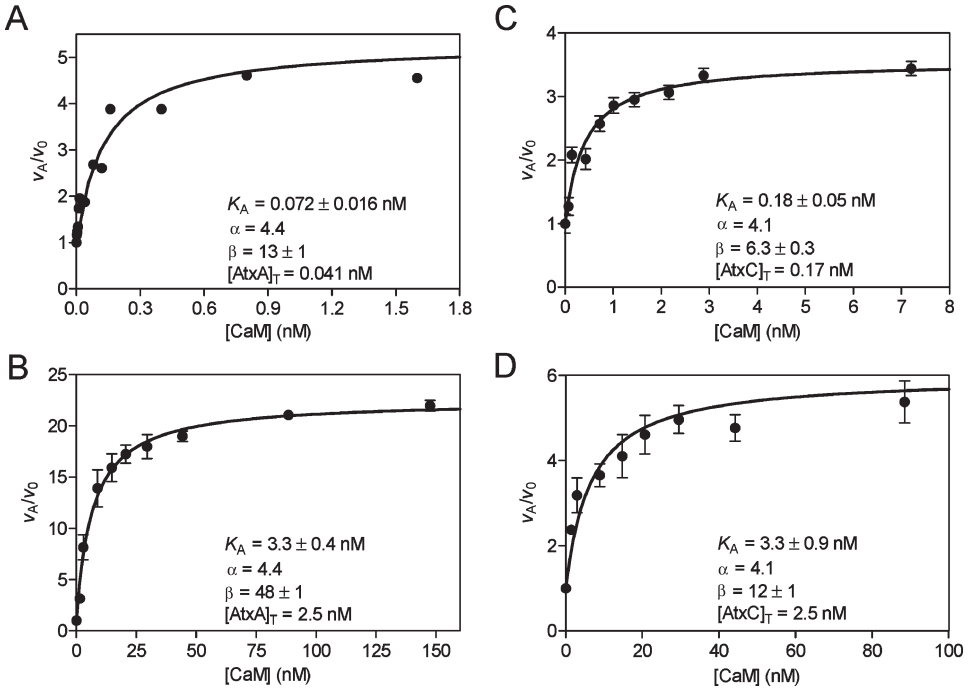

FIGURE 6: Activation profiles of Atxs by CaM under nonreducing and cytosol-like conditions. AtxA or AtxC was incubated for 20 min in the absence or presence of increasing concentrations of CaM under nonreducing conditions [50 mM Tris-HCl (pH 7.4), 50 mM KCl, and 1 mM $CaCl_2$] (A and C) or under reducing conditions [50 mM Tris-HCl (pH 7.4), 18 mM NaCl, 135 mM KCl, 1 mM $CaCl_2$, 9.86 mM reduced glutathione, and 0.14 mM oxidized glutathione] (B and D). The reaction progress curves of phospholipid hydrolysis (1.4 μM PyPG) were followed in 96-well plates on a Safire^2 microplate reader (C and D) or in quartz cuvettes in a Perkin-Elmer LS50B spectrometer at 25 °C (A and B). The general modifier model (eq 2) was fitted to initial rates plotted as v_A/v_0 vs CaM concentration treating the parameter α determined from the specific velocity plot as a constant. Best-fit values of K_A and β as well as enzyme concentrations used in each assay are given in the plots.

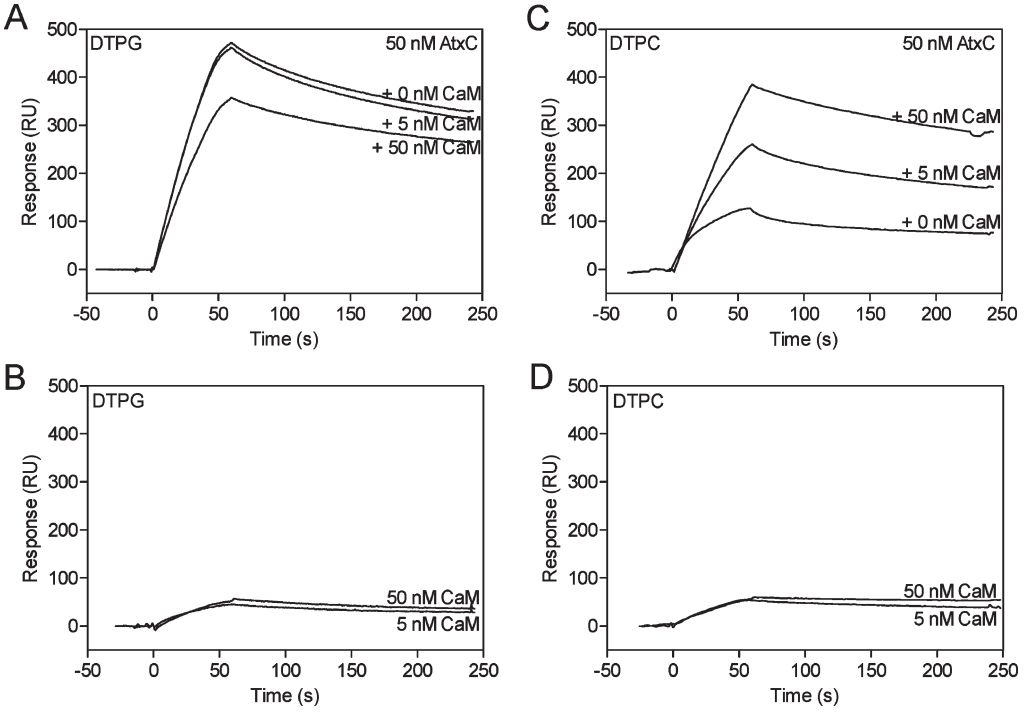

FIGURE 7: CaM changes the membrane binding properties of AtxC. Large unilamellar vesicles of nonhydrolyzable anionic DTPG (A and B) and zwitterionic DTPC (C and D) were immobilized on a Pioneer L1 sensor chip. Mixtures of different concentrations of CaM with 50 nM AtxC (A and C) or CaM alone (B and D) in 10 mM Hepes (pH 7.4), 150 mM NaCl, and 0.5 mM $CaCl_2$ were injected over the immobilized vesicles for 60 s, after which the dissociation was monitored for the next 180 s. Binding curves displayed on sensorgrams were corrected for background obtained by injection of buffer alone.

as AtxC (*29*). Using alternative activity assays, we demonstrated that the potentiation of the enzymatic activity of Atxs by CaM is independent of phospholipid vesicle composition.

Our results indicate that Atxs are not inactivated when exposed to cytosol-like conditions but rather undergo a slow transition to a state with a lower activity (Atx^R). When the

nonreducing conditions are restored, the Atx^R molecules rapidly revert to the more active state (Atx^0). In the presence of CaM, however, the enzymatic activity of both Atx^0 and Atx^R increases to a similar value, in a manner independent of the redox potential. This indicates that binding of CaM triggers a transition of both Atx^0 and Atx^R to a structurally similar state (Atx−CaM) with almost identical phospholipase activity. This $sPLA_2$ stabilizing effect of CaM also explains the higher levels of activation of Atxs by CaM under reducing than under nonreducing conditions. As summarized schematically in Figure 8, our results suggest that Atxs can rotate between three different states, depending on the redox potential and the presence of CaM. Structural changes can be reflected by changes in the intrinsic Trp fluorescence in proteins (*39*). The shift of the intrinsic Trp fluorescence maximum of the AtxA(F24W) mutant from 360 to 380 nm is an indication that the transition between states Atx^0 and Atx^R involves structural rearrangement in the Atx molecule. The intrinsic Trp fluorescence was, however, not affected in a reducing environment when AtxA(F24W) was in the complex with CaM, indicating that the immediate environment of Trp24 remains unchanged. Clearly, CaM increases the conformational stability of Atx in a reducing environment, thus effectively preventing the transition of the enzyme to a state of lower enzymatic activity.

The dependence of the initial rates of hydrolysis of PG vesicles on the concentration of free Ca^{2+} demonstrated that binding to CaM does not affect the apparent affinity of AtxC for Ca^{2+}. Given that the apparent Ca^{2+} affinity values determined in such a manner are dependent on the effects of binding of AtxC to the membrane surface, the binding of a monomeric substrate molecule to the active site of AtxC, and the affinity of AtxC for the

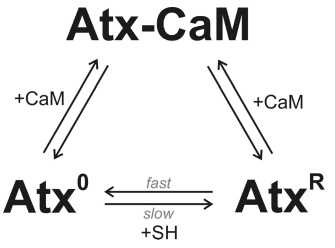

FIGURE 8: CaM stabilizes the structure of Atx. Under nonreducing conditions, Atx exists in conformation Atx^0. Exposure of Atx^0 to reducing conditions causes a gradual shift toward the less active Atx^R form. The Atx^R form rapidly returns to the Atx^0 form in a nonreducing milieu. In a manner independent of environmental conditions, binding of CaM to either Atx^0 or Atx^R induces a transition of the $sPLA_2$ molecules into a highly active CaM-bound form.

Ca^{2+} ion (*37*), we conclude that the changes in these processes caused by CaM binding to AtxC have been collectively compensated. Binding of CaM significantly enhances the catalytic activity of Atxs, and as shown by our kinetic analysis, the mechanism of nonessential activation is valid for both Atxs under both nonreducing and reducing conditions. The coefficients α and β in the general modifier mechanism show that CaM binding affects the catalytic properties of Atxs as well as their affinity for the substrate. In particular, the catalytic efficacy of the enzymes is enhanced ($\beta > 1$), whereas the overall affinity for PG as the substrate is reduced ($\alpha > 1$). The value of the parameter β obtained under reducing, cytosol-like conditions is higher than that obtained under nonreducing conditions, in agreement with the fact that the activation effect is more pronounced under reducing than under nonreducing conditions. This can be explained by the differences in activity between the noncomplexed forms of Atxs, Atx^R and Atx^0, which then, following the association with CaM, again adopt similar conformations. It is conceivable that some more exposed disulfide bonds are split in Atx^R. This reduces the activity of the $sPLA_2$ but, clearly, does not cause complete inactivation, in line with the results obtained with the homologous bovine pancreatic $sPLA_2$ (*42*). When each of the seven disulfides in bovine pancreatic $sPLA_2$ was separately replaced with a pair of alanines, most of the double mutants exhibited only modest changes in conformational stability. Only the C11A/C77A mutant exhibited a large decrease in stability, while the C84A/C96A mutant could not be produced. The enzymatic activities of the bovine pancreatic $sPLA_2$ mutants were not affected significantly (< 10-fold), the exception being the C29A/C45A mutant which underwent a 20-fold decrease in enzyme activity (*7*, *42*).

The mechanism of nonessential activation of AtxA and AtxC on PG vesicles by CaM suggests that the binding affinity of the complex for PG vesicles is reduced relative to that of Atx alone ($\alpha > 1$). This was confirmed by SPR measurements on DTPG vesicles, where the AtxC−CaM complex bound less strongly to immobilized vesicles than AtxC alone. The likely explanation is the difference in the phospholipid interaction surfaces between AtxC and the AtxC−CaM complex. The interfacial binding surface of Atxs is rich in basic and aromatic amino acid residues (*29*), which may be partly covered in the complex by the molecule of CaM with an overall negative charge. A more polar and anionic membrane-binding surface of the complex would result in a lower avidity of the complex for the anionic PG surface. In accordance with our explanation of a reduced level of binding of the complex to anionic surfaces, the opposite effect

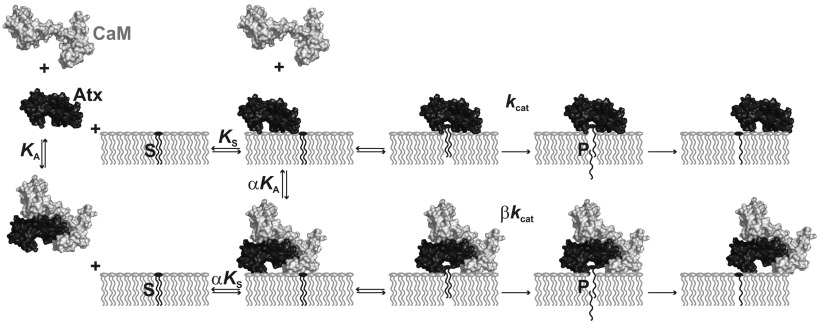

FIGURE 9: Structural−mechanistic relationships of the CaM−Atx interactions. On binding to Atx, CaM modulates the association of Atx with the lipid membrane and its catalytic step, as described by the general modifier mechanism. On the PG vesicle surface, the AtxA−CaM complex binds with a lower affinity than AtxA alone ($\alpha > 1$). A change in the enzyme turnover rate is reflected in the parameter β. On the PG vesicles, the turnover rate of the AtxA−CaM complex is increased in comparison with that of AtxA ($\beta > 1$).

was detected with the complex on zwitterionic PC vesicles. In this case, the binding of the complex was stronger. This is clearly one of the reasons for the stronger activation of AtxC in the presence of CaM on PC than on PG vesicles.

Both Atxs had considerably higher affinity for CaM under nonreducing than under cytosol-like conditions in which the K_A values were in the low nanomolar range. The low K_A values indicate that, under the conditions used, CaM bound tightly to Atxs. K_A for the interaction of AtxC with CaM under nonreducing conditions was 50-fold lower than that determined previously by homologous competition of [^{125}I]AtxC binding to CaM (*43*). This is probably due to the presence of an aggregated phospholipid substrate in kinetic experiments (*38*). Although the affinity of Atxs for CaM is much lower under reducing than nonreducing conditions, Atx molecules nevertheless bind to CaM after translocation into the cytosol of a living cell (*20*). This is in agreement with the fact that the cytosolic concentration of CaM is in the micromolar range (*44*). A (patho)physiologically relevant conclusion of our results is that the activity of Atxs complexed with CaM in the cytosol should be very similar to their activity in the presence of CaM in a nonreducing environment. That would explain the destruction of subcellular structures in nerve cells, for example, mitochondria and synaptic vesicles, following the internalization of Atxs into their cytosol (*19*−*21*).

It is well-established that binding of sPLA$_2$s to the surface of an aggregated substrate, such as membranes or micelles, leads to interfacial activation, i.e., a substantial increase in their enzymatic activity, indicating coupling between the catalytic and interfacial binding events (*45*). The phenomenon has been related to an allosteric effect of the interface on substrate binding to the catalytic site (K_S* allostery) and an effect of specific charge compensation events at the interface on the chemical step (k_{cat}* allostery) (*46*, *47*). These data provide evidence that interfacial activation of sPLA$_2$s, despite their rigid structure stabilized by numerous disulfide bonds, may involve subtle, but functionally significant, conformational changes in the enzyme, rather than structural changes in the substrate. The nonessential activation by CaM can thus be interpreted as a consequence of several possible effects: subtle conformational changes of sPLA$_2$ in the complex, resulting in increased catalytic efficiency, possibly, but not necessarily, related to an increased affinity of the membrane-bound enzyme for a monomeric substrate molecule. Additionally, the interaction of sPLA$_2$ with the membrane surface in the complex may be altered in a way that positively influences the catalytic efficiency through allosteric effects of the interface (Figure 9).

ACKNOWLEDGMENT

Surface plasmon resonance experiments were performed at the Infrastructural Centre for Surface Plasmon Resonance at the Department of Biology, Biotechnical Faculty, University of Ljubljana. We are grateful to Dr. David C. Wilton for the expression plasmid encoding rat liver FABP and to Dr. Roger H. Pain for critical reading of the manuscript.

REFERENCES

1. Schaloske, R. H., and Dennis, E. A. (2006) The phospholipase A$_2$ superfamily and its group numbering system. *Biochim. Biophys. Acta 1761*, 1246–1259.
2. Lambeau, G., and Gelb, M. H. (2008) Biochemistry and physiology of mammalian secreted phospholipases A$_2$. *Annu. Rev. Biochem. 77*, 495–520.
3. Kini, R. M., Ed. (1997) in Venom phospholipase A$_2$ enzymes, structure, function and mechanism , pp 1−511, John Wiley & Sons, Chichester, U.K.
4. Križaj, I., Turk, D., Ritonja, A., and Gubenšek, F. (1989) Primary structure of ammodytoxin C further reveals the toxic site of ammodytoxin. *Biochim. Biophys. Acta 999*, 198–202.
5. Križaj, I., Liang, N. S., Pungerčar, J., Štrukelj, B., Ritonja, A., and Gubenšek, F. (1992) Amino acid and cDNA sequences of a neutral phospholipase A$_2$ from the long-nosed viper (*Vipera ammodytes ammodytes*) venom. *Eur. J. Biochem. 204*, 1057–1062.
6. Pungerčar, J., and Križaj, I. (2007) Understanding the molecular mechanism underlying the presynaptic toxicity of secreted phospholipases A$_2$. *Toxicon 50*, 871–892.
7. Berg, O. G., Gelb, M. H., Tsai, M.-D., and Jain, M. K. (2001) Interfacial enzymology: The secreted phospholipase A$_2$-paradigm. *Chem. Rev. 101*, 2613–2653.
8. Scott, D. L., White, S. P., Otwinowski, Z., Yuan, W., Gelb, M. H., and Sigler, P. B. (1990) Interfacial catalysis: The mechanism of phospholipase A$_2$. *Science 250*, 1541–1546.
9. Yu, B.-Z., Rogers, J., Nicol, G. R., Theopold, K. H., Seshadri, K., Vishweshwara, S., and Jain, M. K. (1998) Catalytic significance of the specificity of divalent cations as K_S* and k_{cat}* cofactors for secreted phospholipase A$_2$. *Biochemistry 37*, 12576–12587.
10. Yu, B. Z., Berg, O. G., and Jain, M. K. (1993) The divalent cation is obligatory for the binding of ligands to the catalytic site of secreted phospholipase A$_2$. *Biochemistry 32*, 6485–6492.
11. Ghomashchi, F., Yu, B.-Z., Berg, O. G., Jain, M. K., and Gelb, M. H. (1991) Interfacial catalysis by phospholipase A$_2$: Substrate specificity in vesicles. *Biochemistry 30*, 7318–7329.
12. Habermann, E., and Jentsch, J. (1967) Sequence analysis of melittin from tryptic and peptic degradation products. *Hoppe-Seyler's Z. Physiol. Chem. 348*, 37–50.
13. Clark, M. A., Özgür, L. E., Conway, T. M., Dispoto, J., Crooke, S. T., and Bomalaski, J. S. (1991) Cloning of a phospholipase A$_2$-activating protein. *Proc. Natl. Acad. Sci. U.S.A. 88*, 5418–5422.
14. Cajal, Y., and Kumar Jain, M. (1997) Synergism between mellitin and phospholipase A$_2$ from bee venom: Apparent activation by intervesicle exchange of phospholipids. *Biochemistry 36*, 3882–3893.
15. Chin, D., and Means, A. R. (2000) Calmodulin: A prototypical calcium sensor. *Trends Cell Biol. 10*, 322–328.
16. Clapham, D. E. (2007) Calcium signalling. *Cell 131*, 1047–1058.
17. Moskowitz, N., Shapiro, L., Schook, W., and Puszkin, S. (1983) Phospholipase A$_2$ modulation by calmodulin, prostaglandins and cyclic nucleotides. *Biochem. Biophys. Res. Commun. 115*, 94–99.
18. Moskowitz, N., Andrés, A., Silva, W., Shapiro, L., Schook, W., and Puszkin, S. (1985) Calcium-dependent binding of calmodulin to phospholipase A$_2$ subunits induces enzymatic activation. *Arch. Biochem. Biophys. 241*, 413–417.
19. Logonder, U., Križaj, I., Rowan, G. E., and Harris, J. B. (2008) Neurotoxicity of ammodytoxin A in the envenoming bites of *Vipera ammodytes ammodytes*. *J. Neuropathol. Exp. Neurol. 67*, 1011–1019.
20. Jenko Pražnikar, Z., Kovačič, L., Rowan, G. E., Romih, R., Rusmini, P., Poletti, A., Križaj, I., and Pungerčar, J. (2008) A presynaptically toxic secreted phospholipase A$_2$ is internalized into motoneuron-like cells where it is rapidly translocated into the cytosol. *Biochim. Biophys. Acta 1783*, 1129–1139.
21. Logonder, U., Jenko-Pražnikar, Z., Scott-Davey, T., Pungerčar, J., Križaj, I., and Harris, J. (2009) Ultrastructural evidence for the uptake of a neurotoxic snake venom phospholipase A$_2$ into mammalian motor nerve terminals. *Exp. Neurol. 219*, 591–594.
22. Gubenšek, F., Ritonja, A., Zupan, J., and Turk, V. (1980) Basic proteins of *Vipera ammodytes* venom. Studies of structure and function. *Period. Biol. 82*, 443–447.
23. Petan, T., Križaj, I., Gubenšek, F., and Pungerčar, J. (2002) Phenylalanine-24 in the N-terminal region of ammodytoxins is important for both enzymic activity and presynaptic toxicity. *Biochem. J. 363*, 353–358.
24. Worrall, A. F., Evans, C., and Wilton, D. C. (1991) Synthesis of a gene for rat liver fatty acid-binding protein and its expression in *Escherichia coli*. *Biochem. J. 278*, 365–368.
25. Radvanyi, F., Jordan, L., Russo-Marie, F., and Bon, C. (1989) A sensitive and continuous fluorometric assay for phospholipase A$_2$ using pyrene-labeled phospholipids in the presence of serum albumin. *Anal. Biochem. 177*, 103–109.
26. Leslie, C. C., and Gelb, M. H. (2004) Assaying phospholipase A$_2$ activity. *Methods Mol. Biol. 284*, 229–242.
27. Hwang, C., Sinskey, A. J., and Lodish, H. F. (1992) Oxidized redox state of glutathione in the endoplasmic reticulum. *Science 257*, 1496–1502.

28. Wilton, D. C. (1990) A continuous fluorescence displacement assay for the measurement of phospholipase A_2 and other lipases that release long-chain fatty acids. *Biochem. J. 266*, 435–439.
29. Petan, T., Križaj, I., Gelb, M. H., and Pungerčar, J. (2005) Ammodytoxins, potent presynaptic neurotoxins, are also highly efficient phospholipase A_2 enzymes. *Biochemistry 44*, 12535–12545.
30. Hixon, M. S., Ball, A., and Gelb, M. H. (1998) Calcium-dependent and -independent interfacial binding and catalysis of cytosolic group IV phospholipase A_2. *Biochemistry 37*, 8516–8526.
31. Botts, J., and Morales, M. (1953) Analytical description of the effects of modifiers and of enzyme multivalency upon the steady state catalyzed reaction rate. *Trans. Faraday Soc. 49*, 696–707.
32. Topham, C. M., and Brocklehurst, K. (1992) In defence of the general validity of the Cha method of deriving rate equations. The importance of explicit recognition of the thermodynamic box in enzyme kinetics. *Biochem. J. 282*, 261–265.
33. Baici, A. (1981) The specific velocity plot. A graphical method for determining inhibition parameters for both linear and hyperbolic enzyme inhibitors. *Eur. J. Biochem. 119*, 9–14.
34. Petan, T., Križaj, I., and Pungerčar, J. (2007) Restoration of enzymatic activity in a Ser-49 phospholipase A_2 homologue decreases its Ca^{2+}-independent membrane-damaging activity and increases its toxicity. *Biochemistry 46*, 12795–12809.
35. Anderluh, G., Beseničar, M., Kladnik, A., Lakey, J. H., and Maček, P. (2005) Properties of nonfused liposomes immobilized on an L1 Biacore chip and their permeabilization by a eukaryotic pore-forming toxin. *Anal. Biochem. 344*, 43–52.
36. Šribar, J., Čopič, A., Pariš, A., Sherman, N. E., Gubenšek, F., Fox, J. W., and Križaj, I. (2001) A high-affinity acceptor for phospholipase A_2 with neurotoxic activity is a calmodulin. *J. Biol. Chem. 276*, 12493–12496.
37. Singer, A. G., Ghomashchi, F., Le Calvez, C., Bollinger, J., Bezzine, S., Rouault, M., Sadilek, M., Nguyen, E., Lazdunski, M., Lambeau, G., and Gelb, M. H. (2002) Interfacial kinetic and binding properties of the complete set of human and mouse groups I, II, V, X, and XII secreted phospholipases A_2. *J. Biol. Chem. 277*, 48535–48549.
38. Lathrop, B., Gadd, M., Biltonen, R. L., and in Rule, G. S. (2001) Changes in Ca^{2+} affinity upon activation of *Agkistrodon piscivorus piscivorus* phospholipase A_2. *Biochemistry 40*, 3264–3272.
39. Petrovič, U., Šribar, J., Pariš, A., Rupnik, M., Kržan, M., Vardjan, N., Gubenšek, F., Zorec, R., and Križaj, I. (2004) Ammodytoxin, a neurotoxic secreted phospholipase A_2, can act in the cytosol of the nerve cell. *Biochem. Biophys. Res. Commun. 324*, 981–985.
40. Logonder, U., Jorgačevski, J., Anderluh, G., Petrovič, U., Poberaj, I., and Križaj, I. (2008) A secreted phospholipase A_2 binds to calmodulin at sub-micromolar concentrations of calcium. *Acta Chim. Slov. 55*, 541–546.
41. Alston, R. W., Urbanikova, L., Sevcik, J., Lasagna, M., Reinhart, G. D., Scholtz, J. M., and Pace, C. N. (2004) Contribution of single tryptophan residues to the fluorescence and stability of ribonuclease Sa. *Biophys. J. 87*, 4036–4047.
42. Zhu, H.-X., Dupureur, C. M., Zhang, X.-Y., and Tsai, M. D. (1995) Phospholipase A_2 engineering. The roles of disulfide bonds in structure, conformational stability, and catalytic function. *Biochemistry 34*, 15307–15314.
43. Prijatelj, P., Šribar, J., Ivanovski, G., Križaj, I., Gubenšek, F., and Pungerčar, J. (2003) Identification of a novel binding site for calmodulin in ammodytoxin A, a neurotoxic group IIA phospholipase A_2. *Eur. J. Biochem. 270*, 3018–3025.
44. De Haro, L., Quetglas, S., Iborra, C., Leveque, C., and Seagar, M. (2003) Calmodulin-dependent regulation of a lipid binding domain in the v-SNARE synaptobrevin and its role in vesicular fusion. *Biol. Cell 95*, 459–464.
45. Jain, M. K., and Berg, O. G. (1989) The kinetics of interfacial catalysis by phospholipase A_2 and regulation of interfacial activation: Hopping versus scooting. *Biochim. Biophys. Acta 1002*, 127–156.
46. Berg, O. G., Yu, B.-Z., and Jain, M. K. (2009) Thermodynamic reciprocity of the inhibitor binding to the active site and the interface binding region of IB phospholipase A_2. *Biochemistry 48*, 3209–3218.
47. Yu, B.-Z., Bai, S., Berg, O. G., and Jain, M. K. (2009) Allosteric effect of amphiphile binding to phospholipase A_2. *Biochemistry 48*, 3219–3229.